

Hermite interpolation of ruled surfaces and channel surfaces

Boris Odehnal

University of Applied Arts Vienna

December 13, 2017

Abstract

We show an algebraic way to interpolate Hermite data of ruled or channel surfaces by computing polynomial curves within Plücker's and Lie's quadric serving as point models for the geometries of lines and spheres. The Bézier ansatz for a curve in either quadric involves some design parameters guiding the shape of the ruled or channel surface. These parameters are to be determined by solving a system of algebraic equations. Since in our ansatz there are more shape parameters than equations, there are some degrees of freedom which can be used in the design process. The degrees of the equations allow us to predict the number of possible solutions. Together with geometric criteria, useful solutions, *i.e.*, solutions that meet practical requirements can be selected. Our main goal is the interpolation of G^k data at the boundaries of ruled surfaces or channel surfaces. We aim at low degree interpolants.

Key Words: interpolation, Hermite data, ruled surface, channel surface, Plücker's quadric, Lie's quadric, rational normal curve.

MSC (AMS 2010): 97N50, 53A25, 53A99, 53B99, 68W30, 14J26, 51N15.

1 Introduction

There are several algorithms treating interpolation problems with ruled surfaces. Many algorithms focus on developable ruled surfaces, see [14, 18, 19, 29]. In some cases, interpolation of ruled surfaces solves reconstruction tasks and comes along with surface recognition [27, 28].

The most simple case sees a finite sequence of lines that is to be interpolated by a ruled surface, cf. [14, 15, 18, 19, 23, 29]. A polynomial ruled surface that passes through the given lines could also be found with the algorithm presented in [8] by replacing the hypersphere with Plücker's quadric. For practical reasons this may be not sufficient, since a ruled surface that just interpolates a certain number of lines has to be of sufficiently high degree. Therefore, the interpolant will show some unwanted behavior in between the data lines, for example, uncontrolled oscillation or even loops, see Fig. 1. Such a nasty behavior especially occurs when we interpolate data with algebraic ruled surfaces of very high degree.

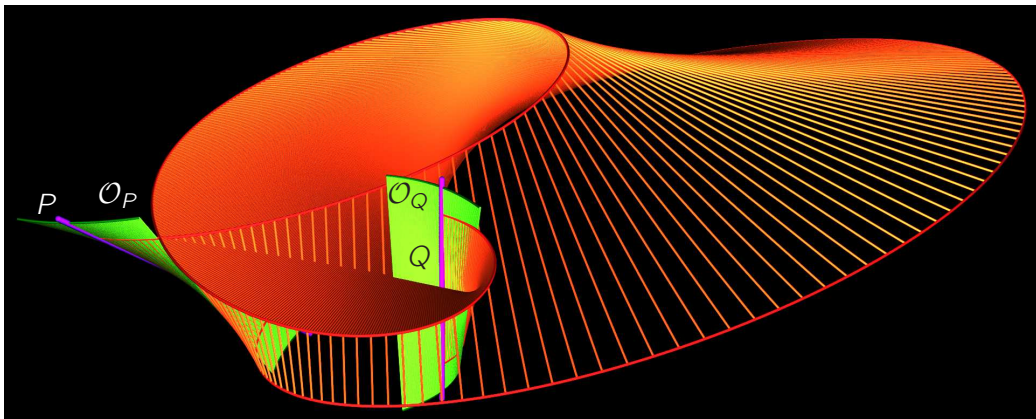


Figure 1: Interpolation of G^2 data: The depicted solution interpolates G^2 data consisting of two osculating reguli \mathcal{O}_P and \mathcal{O}_Q (green) at the boundary rulings P and Q (violet). The solution has a loop and self-intersections in between the boundary data due to the high degree and due to improperly chosen shape parameters.

The interpolation with non-torsal ruled surfaces is only treated in the G^1 case until now, see [26]. In order to glue ruled surface patches with G^1 continuity, it is suggested to adapt the bi-arcs technique as known from planar splines to ruled quadrics by matching contact projectivities along common generators. This resulted in bi-arcs of ruled quadrics and has, however, two disadvantages: 1. An intermediate line has to be inserted. 2. The degree of the interpolants is restricted to two, and thus, torsal rulings or inflection rulings cannot be interpolated properly.

In the following, we shall drop the restrictions on the degree. However, we do not want to raise the degrees of the interpolants too far. Oscillations as can be observed with polynomial functions also occur with algebraic ruled or

channel surfaces of higher degree (cf. Fig. 1). Therefore, we shall use the lowest possible degrees in order to solve certain interpolation problems.

The equivalent interpolation problem for channel surfaces has been attacked using the cyclographic model of sphere geometry in [2]. However, this approach ignores that on the way from the cyclographic model back to the channel surface in \mathbb{R}^3 one degree of smoothness gets lost when differentiating in order to get the envelope (=channel surface) of the one-parameter family of spheres.

As we shall see in Sec. 3, the interpolation of G^1 data on quadrics can be done by means of cubic curves in general. Raising the degree of the G^1 interpolant to four could either lead to more flexibility (since there is one more control point) or to more precision (since the control points can be determined such that we gain a C^1 transition). We shall discuss this in more detail in Sec. 5. However, in this case we have no guarantee for real solutions.

Interpolation of G^2 and G^3 data is more fascinating, challenging, and perhaps of more practical relevance since higher smoothness of interpolants makes them useful for many design purposes. A G^3 transition between two surfaces is highly desirable. Shiny surfaces composed of G^3 patches show reflection lines and isophotes with G^2 smoothness at the transition curves, see Fig. 2.

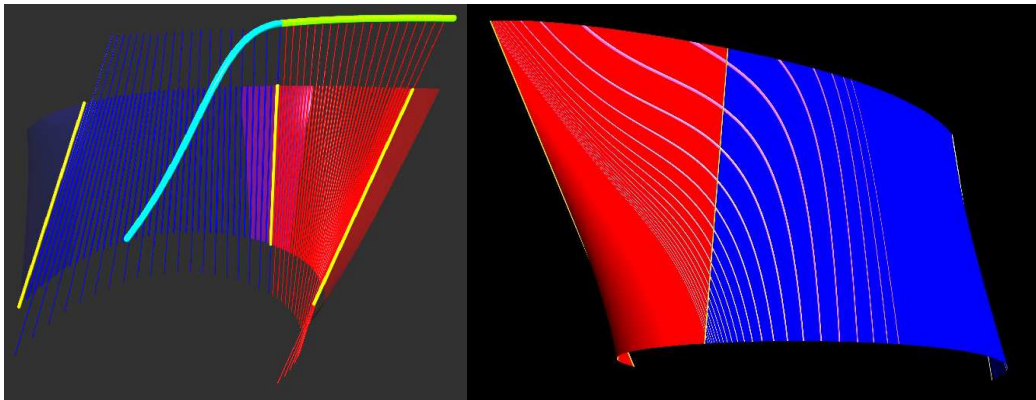


Figure 2: At a G^3 transition between two ruled surface patches, even the curve of flecnodes (only one branch is shown) turns out to be at least of smoothness G^0 (left: discrete version with curve of flecnodes; right: smooth surface patches with some reflection lines showing a G^2 link at the transition from one patch to the other).

Until now, we have put emphasis on the interpolation of ruled surface data in \mathbb{R}^3 . An old and well-known result from classical geometry states that the

geometry of lines in three-space is more or less the same as the geometry of spheres in Euclidean three-space, see [5, 31, 32]. Both geometries are four-dimensional and can be modeled on quadrics as we shall see in Sec. 2.

Thus, interpolation problems in both geometries can be reformulated as interpolation problems in quadrics. Although there are algorithms for such tasks, see for example [6, 7, 8, 11], we go a different way in order to find exact polynomial parametrizations of the interpolants with lowest algebraic degree. Inserting the polynomial representation (preferably, the Bézier representation) into the quadric's equation results in a polynomial that has to vanish for all parameter values. Therefore, all the polynomial's coefficients have to vanish and this yields a system of polynomial equations. This allows us to determine the control points of the polynomial interpolant. The interpolation by means of developable ruled surfaces can also be done this way. We just have to impose further algebraic conditions on the Bézier representation of the interpolants and the endpoint data has to fulfill some conditions.

In Sec. 2, we collect all necessary facts on line and sphere geometry in order to make the computations understandable. The various kinds of contacts between two ruled or channel surfaces shall be explained roughly. For details we refer to the classical literature. The geometry of spheres and channel surfaces can be treated in a similar way. Sec. 2 also provides an overview on the geometry of spheres and channel surfaces. In Sec. 3, we study Bézier curves in quadrics and treat the *line geometric* and the *sphere geometric* case in a uniform way. This enables us to give the algebraic systems of equations that have to be solved in order to compute the interpolants to given boundary data for ruled surfaces as well as for channel surfaces. Sec. 4 describes the algorithms and collects the main results. We give examples and show how the presented interpolation technique works. Finally, we conclude in Sec. 5 and add some more material. We discuss alternative approaches to the various interpolation problems.

2 Klein's quadric and Lie's quadric

We deal with lines and spheres in the Euclidean three-space \mathbb{R}^3 where we use Cartesian coordinates (x, y, z) . Whenever necessary, we switch to the complex extension and to the projective closure.

2.1 Line geometry

We give just a very brief overview and results as far as they are necessary in order to understand the computations and considerations. For details, we refer to the classical literature, such as [10, 11, 22, 30, 31, 32, 33].

A straight line $L \subset \mathbb{R}^3$ shall be represented by its Plücker coordinates $(\mathbf{l}, \bar{\mathbf{l}}) \in \mathbb{R}^6 \setminus \{\mathbf{o}\}^1$ where $\mathbf{l} = (l_1, l_2, l_3) \in \mathbb{R}^3$ is a *direction vector* and $\bar{\mathbf{l}} = (l_4, l_5, l_6) \in \mathbb{R}^3$ is the line's *momentum vector*. Assume that the line L is spanned by two different points P and Q with Cartesian coordinate vectors \mathbf{p} and \mathbf{q} . Then, we write $L = [P, Q]$ and the Plücker coordinates are given by

$$\mathbf{l} = \mathbf{q} - \mathbf{p}, \quad \bar{\mathbf{l}} = \mathbf{p} \times \mathbf{q} \quad (1)$$

where $\times : \mathbb{R}^3 \times \mathbb{R}^3 \rightarrow \mathbb{R}^3$ indicates the canonical exterior product of vectors in \mathbb{R}^3 induced by the canonical scalar product $\langle \cdot, \cdot \rangle : \mathbb{R}^3 \times \mathbb{R}^3 \rightarrow \mathbb{R}$. Here, L is oriented, *i.e.*, \mathbf{l} points from P to Q . From (1) it is clear that

$$2\langle \mathbf{l}, \bar{\mathbf{l}} \rangle = 0 =: \Omega^L(L, L) \quad (2)$$

holds for the Plücker coordinates of any line in \mathbb{R}^3 . We will not introduce a further symbol for the Plücker coordinates of a line L (or the Lie coordinates of a sphere S) in order not to overload the notation. So, we shall sometimes write $\Omega^L(X, Y)$, or later, $\Omega^S(S, T)$ for the value of the particular bilinear form taken on the respective pairs of vectors in \mathbb{R}^6 .

On the other hand, any pair of vectors $(\mathbf{l}, \bar{\mathbf{l}}) \in \mathbb{R}^6 \setminus \{\mathbf{o}\}$ that satisfies (2) can be interpreted as Plücker coordinates of a line L in three-space, see [11, 31]. Any scalar multiple $(\lambda\mathbf{l}, \lambda\bar{\mathbf{l}})$ with $\lambda \in \mathbb{R}^*$ describes the same line in $L \subset \mathbb{R}^3$ (or even in \mathbb{P}^3) which allows us to interpret $(\mathbf{l}, \bar{\mathbf{l}})$ as homogeneous coordinates of a point L in projective five-space $\mathbb{P}^5(\mathbb{R})$. However, the orientation of lines gets lost if we change to homogeneous coordinates. Henceforth, L means either the line in \mathbb{R}^3 (or in \mathbb{P}^3) or the corresponding point in \mathbb{P}^5 .

Although we have started with oriented lines in Euclidean three-space, Plücker coordinates can also be used to describe lines at infinity. Such lines are given by $\mathbf{l} = \mathbf{o}$ while $\bar{\mathbf{l}} \neq \mathbf{o}$. Lines through the origin of the coordinate system are characterized by $\bar{\mathbf{l}} = \mathbf{o}$ while $\mathbf{l} \neq \mathbf{o}$. The transition from inhomogeneous Cartesian coordinates in \mathbb{R}^3 to homogeneous coordinates does not affect (2). If $\mathbf{x} = (x_1, x_2, x_3)$ and $\bar{\mathbf{x}} = (x_4, x_5, x_6)$, then

$$M_2^4 : \frac{1}{2}\Omega^L(X, X) = \langle \mathbf{x}, \bar{\mathbf{x}} \rangle = x_1x_4 + x_2x_5 + x_3x_6 = 0 \quad (3)$$

¹We use the symbol \mathbf{o} for the zero vector in any vector space.

is the equation of a quadratic hypersurface M_2^4 in projective five-space \mathbb{P}^5 all of whose points correspond to lines in \mathbb{P}^3 , and *vice versa*. M_2^4 is of index two which means that the maximal subspaces (of \mathbb{P}^5) contained in M_2^4 are planes. There are two kinds of planes in M_2^4 : Those of the first kind correspond to stars of lines in \mathbb{P}^3 ; those of the second kind correspond to ruled planes in \mathbb{P}^3 . The quadric M_2^4 is covered by two three-parameter manifolds of planes and contains a five-parameter manifold of lines corresponding to the pencils of lines in \mathbb{P}^3 .

$\Omega^L(X, Y)$ is the polar form of M_2^4 and assigns to each point $X \in \mathbb{P}^5$ the polar hyperplane with regard to M_2^4 . Especially, if $X \in M_2^4$, then $\Omega^L(X, Y) = 0$ is the equation of the tangential hyperplane $T_X M_2^4$ of M_2^4 at X . Any two different lines (linearly independent Plücker coordinates) L, M with $\Omega^L(L, M) = 0$ are coplanar, *i.e.*, they are either intersecting in a point or they are parallel.

A C^r ruled surface in \mathbb{P}^3 is a one-parameter family of lines with an r -times differentiable parametrization $\mathcal{R} : I \times \mathbb{P}^1 \rightarrow \mathbb{P}^3$ and can be converted via (1) into a C^r parametrization $\mathcal{R} : I \subset \mathbb{R} \rightarrow M_2^4$ of a curve in M_2^4 . Conversely, each C^r curve in $\mathcal{R} \subset M_2^4$ defines a C^r ruled surface in \mathbb{P}^3 . The interpolation of ruled surfaces can, therefore, be traced back to a curve interpolation problem on the quadric M_2^4 .

Especially, algebraic curves of degree n in M_2^4 correspond to algebraic ruled surfaces of degree n . Among them, we find lines and conics representing pencils of lines and reguli (*i.e.*, the one-parameter families of rulings on quadrics), see [10, 11, 30, 31]. Rational ruled surfaces admit rational parametrizations and can be described by curves in M_2^4 with even polynomial parametrization due to the homogeneity of the Plücker representation.

Since we are dealing with G^k ($k \in \{0, 1, 2, 3\}$) interpolation of ruled surfaces, we should understand the basics of (projective) differential geometry of ruled surfaces (or curves in M_2^4). For details, we refer to [10, 11, 30].

A point $R_0 = \mathcal{R}(t_0)$ is called *regular* if $\dot{R}_0 = \dot{\mathcal{R}}(t_0)$ and R_0 are linearly independent, otherwise R_0 is called *singular*. (In the following, we suppress the precise position $t_0 \in I$ on the curve in order not to overload the notation and write simply R, \dot{R}, \dots instead of R_0, \dot{R}_0, \dots . With a $\dot{}$ we indicate the differentiation with respect to the one and only parameter.)

At a regular point R , the tangent T_1 to the curve $\mathcal{R} \subset M_2^4$ is spanned by the point R and the first derivative point \dot{R} , *i.e.*, $T_1 = [R, \dot{R}]$. The line T_1 is also tangent to M_2^4 . A reparametrization of \mathcal{R} only causes a shift of the derivative point \dot{R} on T_1 which is equivalent to the change of the speed of a particle moving on the curve. The intersection of T_1 's polar space with regard

to M_2^4 is a two-dimensional cone whose points correspond to the lines of the *parabolic linear line congruence* of surface tangents of \mathcal{R} along R , see Fig. 3. This congruence collapses to a ruled plane if $T_1 \cap M_2^4$ or, equivalently, if $\Omega^L(T_1, T_1) = \Omega^L(\dot{R}, \dot{R}) = 0$.² A ruling R is called *torsal* if $\Omega^L(\dot{R}, \dot{R}) = 0$. A ruled surface that consists of torsal rulings only is called a *torsal ruled surface*, is *developable*, and its parametrization $\mathcal{R}(t)$ satisfies $\Omega(\dot{\mathcal{R}}, \dot{\mathcal{R}}) \equiv 0 \forall t \in I$.

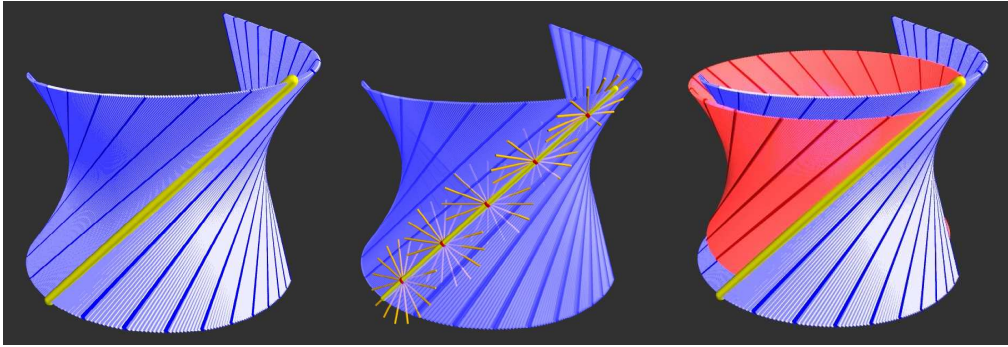


Figure 3: Differential geometric properties of order 0, 1, 2 of a ruled surface (blue) along a regular ruling R (yellow): the ruling (left), the surface tangents along R (middle), the osculating regulus (red) along R (right).

The osculating subspaces T_k of any dimension $k = 0, 1, 2, 3, \dots$ are spanned by the first $k + 1$ derivative points $R^{(k)}$ of \mathcal{R} at R including $R^{(0)} = R$.

Further, the points of $M_2^4 \cap T_2$ correspond to the lines of the *osculating regulus* (see Fig. 3), regularity of the non-torsal ruling R and the linear independence of R, \dot{R}, \ddot{R} provided. The points of M_2^4 which lie in the polar space of T_2 (with regard to M_2^4) correspond to the lines of the complementary regulus on the osculating quadric of \mathcal{R} along R . If $T_2 \subset M_2^4$, then \mathcal{R} behaves locally either like a quadratic cone or a plane.

If the osculating three-spaces of two different curves in M_2^4 agree at some regular non-inflection point P , then the two ruled surfaces share even the flecnodes on the common ruling P , see [24, 30, 33].

2.2 Geometry of spheres

Now, we start and stay in Euclidean three-space \mathbb{R}^3 . We use a coordinatization of the manifold of Euclidean spheres that was used in [32]. There, a

²Note that $\Omega^L(R, R) = \Omega^L(R, \dot{R}) = 0$ for all $t \in I$.

generic sphere S is usually given by its inhomogeneous equation in Cartesian coordinates as

$$S : (s_6 - s_4)(x^2 + y^2 + z^2) - 2s_1x - 2s_2y - 2s_3z + (s_6 + s_4) = 0 \quad (4)$$

where $s_i \in \mathbb{R}$ (for $i \in \{1, \dots, 6\}$) and $s_6 - s_4 \neq 0$ until stated otherwise. It is elementary to verify that the center M of S has the Cartesian coordinates $\mathbf{m} = \frac{1}{s_6 - s_4}(s_1, s_2, s_3)$ and the radius R satisfies $R^2 = \frac{s_1^2 + s_2^2 + s_3^2}{(s_6 - s_4)^2} - (s_6 + s_4)$. We define the fifth coordinate s_5 of the sphere S by letting $R = \frac{s_5}{s_6 - s_4}$ which yields $s_6^2 - s_4^2 - s_1^2 - s_2^2 - s_3^2 = -s_5^2$, and thus,

$$L_2^4 : \frac{1}{2}\Omega^S(S, S) = s_1^2 + s_2^2 + s_3^2 + s_4^2 - s_5^2 - s_6^2 = 0. \quad (5)$$

The sign of R can be used in order to express the sphere's orientation.

Now, we define $\mathbf{s} = (s_1, \dots, s_6) \in \mathbb{R}^6 \setminus \{\mathbf{o}\}$ as the coordinates of the sphere S . It is easy to see that any scalar multiple $\sigma \cdot \mathbf{s} \in \mathbb{R}^6$ with $\sigma \in \mathbb{R}^*$ describes the same sphere, since both, the center M and the radius R are linear rational in s_i and the factor σ can be canceled. Like in the case of the Plücker coordinates of lines, any six-tuple $(s_1, \dots, s_6) \in \mathbb{R}^6 \setminus \{\mathbf{o}\}$ subject to (5) can be interpreted as the homogeneous coordinate vector of a point in projective five-space \mathbb{P}^5 . If the six-tuple satisfies (5), then it corresponds to a point in $L_2^4 \subset \mathbb{P}^5$. On the other hand, any point on L_2^4 corresponds to a sphere in Euclidean three-space \mathbb{R}^3 . However, orientations may be altered when dealing with homogeneous coordinates.

Obviously, the hypersurface $L_2^4 \subset \mathbb{P}^5$ is a quadric; frequently called *Lie's quadric* and it is a point model for the geometry of *oriented spheres* in Euclidean three-space \mathbb{R}^3 . However, L_2^4 differs from M_2^4 over the real number field: It is of index 1, *i.e.*, the maximal subspaces of \mathbb{P}^5 contained in L_2^4 are straight lines. The polar system of L_2^4 also has a geometric meaning. Any pair (S, T) of points conjugate with respect to L_2^4 , *i.e.*, $\Omega^S(S, T) = 0$, corresponds to a pair of spheres in Euclidean three-space being in (oriented) contact.

The hyperplane $s_6 - s_4 = 0$ intersects L_2^4 along the three-dimensional quadratic cone $\Gamma : s_1^2 + s_2^2 + s_3^2 - s_5^2 = 0$ whose points correspond to the (oriented) planes in Euclidean three-space which are then considered as spheres with $R = \infty$. Γ is usually referred to as Blaschke's cone and it is a point model for Laguerre geometry, *i.e.*, the geometry of oriented planes in Euclidean three space, cf. [3, 5, 9]. Points on L_2^4 with $s_5 = 0$ represent spheres with radius 0 which should rather be considered as isotropic cones of Euclidean geometry. Like in case of ruled surfaces, a C^r curve ($r \geq 1$) $\mathcal{C} : I \subset \mathbb{R} \rightarrow L_2^4$ in Lie's quadric represents a one-parameter C^r family of spheres in \mathbb{R}^3 . Usually, such

families of spheres have an envelope which is touched by all spheres along their *characteristic circles*. These envelopes are called *channel surfaces* if the radius of the spheres varies and *pipe surfaces* if the radius is constant. It is worth to point out that the computation of the envelope of a family of spheres needs the process of differentiation. Thus, starting from a G^k interpolant in any point model of sphere geometry, we end with a G^{k-1} envelope. This should always be taken into account when dealing with G^k interpolants in the model space. Moreover, the envelope of a family of spheres needs not be real even though all spheres in the family are real as is the case with a family of concentric spheres. If the algebraic degree of the curve $(\mathbf{m}, R) : I \rightarrow \mathbb{R}^4$ (cyclographic image of the one-parameter family of spheres $\langle \mathbf{x} - \mathbf{m}, \mathbf{x} - \mathbf{m} \rangle = R^2$, see [5, 9, 21]) equals n , then the algebraic degree of the envelope (channel surface) is at most $4n - 2$.

Figure 4 illustrates the differential geometric properties of one-parameter families of spheres up to order two. The top row shows only the one-parameter families of spheres, while the bottom row illustrates the envelopes of the families of spheres, *i.e.*, the channel surfaces.

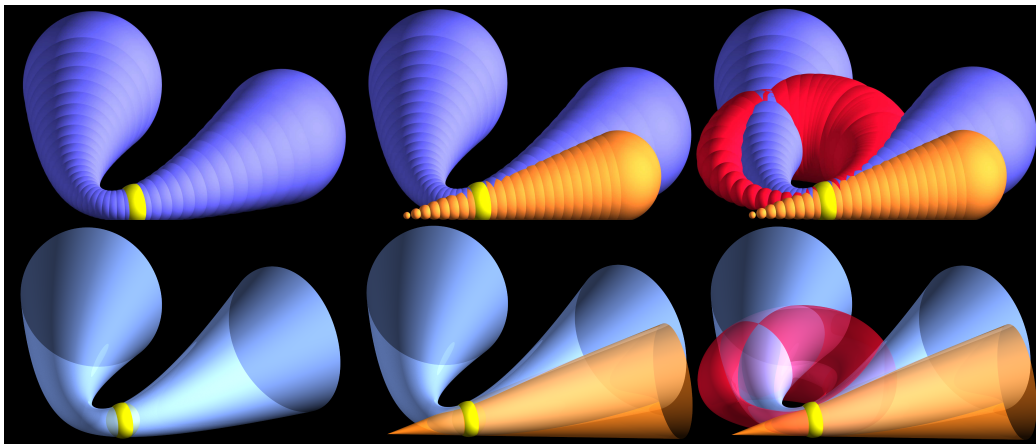


Figure 4: Top row: Differential geometric properties of one-parameter families of spheres. From left to right: G^0 , G^1 , G^2 . Bottom row: the envelopes.

L_2^4 's intersection with the osculating subspaces T_k of $\mathcal{C} \subset L_2^4$ correspond to families of spheres that are in the k -th order contact with the spheres in the family \mathcal{C} , and further, they represent, among others, channel surfaces that are in contact of order $k - 1$ with the envelope of the family of spheres.

Curves in L_2^4 of degrees one and two correspond to special channel surfaces: cones/cylinders (of revolution) and Dupin cyclides.

We shall close this section with the conversion of sphere data into sphere coordinates, points on Lie's quadric L_2^4 . Assume a sphere S has the center M with Cartesian coordinates $\mathbf{m} = (m_1, m_2, m_3)$ and let the radius of the sphere be R . The point in L_2^4 that corresponds to S shall also be denoted by S . We want to find the coordinate vector $\mathbf{s} = (s_1, s_2, s_3, s_4, s_5, s_6)$ of the sphere S . Note that \mathbf{s} is subject to (5) and $s_6 - s_4 \neq 0$, otherwise S is a plane.

First, we observe $m_1(s_6 - s_4) = s_1$, $m_2(s_6 - s_4) = s_2$, $m_3(s_6 - s_4) = s_3$, and $R(s_6 - s_4) = s_5$. The latter four equations can be solved for s_1 , s_2 , s_3 , and s_5 . This results in a two-dimensional subspace of \mathbb{R}^6 with the parametrization

$$V := (m_1(s_6 - s_4), m_2(s_6 - s_4), m_3(s_6 - s_4), s_4, (s_6 - s_4)R, s_6)$$

with $(s_4, s_6) \in \mathbb{R}^2 \setminus \{\mathbf{o}\}$. Now, $\Omega^S(V, V) = 0$ yields

$$s_4 : s_6 = (R^2 - \langle \mathbf{m}, \mathbf{m} \rangle + 1) : (R^2 - \langle \mathbf{m}, \mathbf{m} \rangle - 1)$$

which finally results in

$$\mathbf{s} = (2m_1, 2m_2, 2m_3, \langle \mathbf{m}, \mathbf{m} \rangle - R^2 - 1, 2R, \langle \mathbf{m}, \mathbf{m} \rangle - R^2 + 1). \quad (6)$$

The latter equation is that of the stereographic projection from the cyclographic model to Lie's quadric.

3 Bézier curves within quadrics

We will not use the algorithm offered in [8], since it only returns interpolants on a collection of points (without any further information on derivatives there). The idea from [16] cannot be applied directly to problems in higher dimensional spaces. The techniques developed in [17] or [25] can only be applied once a channel surface is known. The interpolation with cyclide patches is well understood, see [20], but it restricts to a certain very stiff class of channel surfaces.

We assume that $\Omega : \mathbb{R}^6 \times \mathbb{R}^6 \rightarrow \mathbb{R}$ is a non-degenerate symmetric bilinear form on \mathbb{R}^6 . It could be either one of the forms Ω^L and Ω^S from (3) and (5) or any other. Naturally, $\mathcal{Q} : \Omega(\mathbf{x}, \mathbf{x}) = 0$ is the equation of a regular quadric in \mathbb{P}^5 whose polar system is described by the polar form Ω .

Let $\mathcal{B} : I \subset \mathbb{R} \rightarrow \mathbb{R}^6$ be a C^r parametrization of a curve with sufficiently large $r \in \mathbb{N}$. For the sake of simplicity, we use the symbol \mathcal{B} for the curve as well as for its parametrization. If the curve is entirely contained in the quadric, then

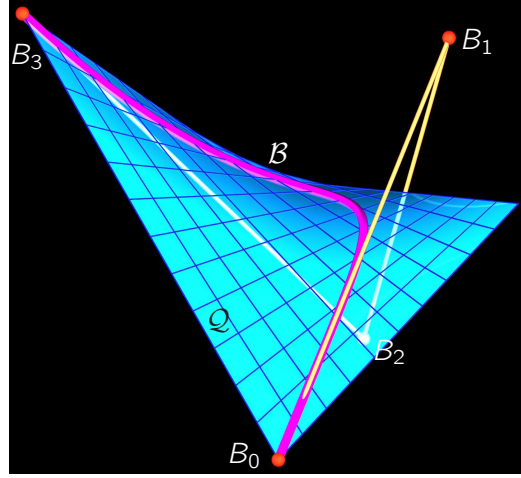


Figure 5: Bézier curve \mathcal{B} in a quadric with its control polygon.

the parametrization annihilates the quadric's equation and so $\Omega(\mathcal{B}, \mathcal{B}) \equiv 0$ holds in I . Differentiation with respect to t yields the following identities

$$\Omega(\mathcal{B}, \dot{\mathcal{B}}) \equiv 0, \quad \Omega(\mathcal{B}, \ddot{\mathcal{B}}) + \Omega(\dot{\mathcal{B}}, \dot{\mathcal{B}}) \equiv 0, \quad 3\Omega(\dot{\mathcal{B}}, \ddot{\mathcal{B}}) + \Omega(\mathcal{B}, \ddot{\mathcal{B}}) \equiv 0, \quad \dots \quad (7)$$

In the following, when we deal with interpolation tasks, we always have boundary data $D_0 := [P, \dot{P}, \ddot{P}, \dots]$ and $D_1 := [Q, \dot{Q}, \ddot{Q}, \dots]$ which comes either from one or two ruled surface(s) or channel surface(s) and satisfies (7). In any case, D_0 and D_1 shall be the boundary data of the interpolant that admits a polynomial representation $\mathcal{B} : [0, 1] \subset \mathbb{R} \rightarrow \mathcal{Q}$. This polynomial parametrization is written in the geometrically favorable Bernstein basis, *i.e.*, as a Bézier curve

$$\mathcal{B}(t) = \sum_{k=0}^n \varphi_k \mathbf{b}_k \quad (8)$$

with control points B_k (represented by their homogeneous coordinate vectors \mathbf{b}_k) and with the Bernstein polynomials

$$\varphi_k = \binom{n}{k} (1-t)^{n-k} t^k \quad (\text{with } k \in \{0, 1, \dots, n\}) \quad (9)$$

as basis functions, see [13].

The control points shall be determined such that the given osculating subspaces agree with that of the interpolant:

$$\begin{aligned} \mathcal{B}(0) = P, \quad [\mathcal{B}(0), \dot{\mathcal{B}}(0)] &= [P, \dot{P}], \quad [\mathcal{B}(0), \dot{\mathcal{B}}(0), \ddot{\mathcal{B}}(0)] = [P, \dot{P}, \ddot{P}], \dots, \\ \mathcal{B}(1) = Q, \quad [\mathcal{B}(1), \dot{\mathcal{B}}(1)] &= [Q, \dot{Q}], \quad [\mathcal{B}(1), \dot{\mathcal{B}}(1), \ddot{\mathcal{B}}(1)] = [Q, \dot{Q}, \ddot{Q}], \dots \end{aligned}$$

A Bézier curve $\mathcal{B} : [0, 1] \subset \mathbb{R} \rightarrow \mathbb{R}^6$ is entirely contained in the quadric \mathcal{Q} if, and only if,

$$p(t) := \Omega(\mathcal{B}(t), \mathcal{B}(t)) \equiv 0 \quad (10)$$

holds in I . We assume that $\mathcal{B}(t)$ is a Bézier curve of degree $n \in \mathbb{N}^*$ as given in (8). Then, (10) is a polynomial $p(t) = \sum_{i=0}^{2n} a_i t^i$ in t of degree $2n$ with $2n+1$ coefficients a_0, \dots, a_{2n} depending on the control points B_k . Since (10) has to vanish all over $[0, 1]$, all of its coefficients have to vanish simultaneously. In other words, \mathcal{B} has to have more than $2n$ points of intersection with the quadric $\mathcal{Q} : \Omega(\mathbf{x}, \mathbf{x}) = 0$. This yields $2n+1$ conditions on the control points B_k of the Bézier curve \mathcal{B} .

In order to make the coefficients of $p(t)$ somehow symmetric, we shall write the polynomial also in the Bernstein basis. Therefore, $p(t) = \sum_{i=0}^{2n} a_i \varphi_i$. Since (7) is valid, we can immediately see that the coefficients of $(1-t)^{2n}$, $t(1-t)^{2n-1}$, $t^{2n-1}(1-t)$, and t^{2n} vanish. Thus, the two zeros $t=0$ and $t=1$ of $p(t)$ (both with multiplicity two) are *a priori* known, and hence, the polynomial is divisible by the factor $t^2(1-t)^2$ and the actual degree drops to $2n-4$. The polynomial $p(t) \cdot t^{-2} \cdot (1-t)^{-2}$ has only $2n-3$ coefficients which equals the number of equations to be solved.

Later, we will make use of the abbreviation

$$\Omega_{i,j} := \Omega(\mathbf{b}_i, \mathbf{b}_j)$$

for the value taken by the bilinear form Ω on the pair $(\mathbf{b}_i, \mathbf{b}_j)$ of coordinate vectors representing the pair (B_i, B_j) of base points of the Bézier curve \mathcal{B} .

We shall point out that any (rational) polynomial curve in a ruled quadric is a collinear image of a *rational normal curve*, see [4]. Further, rational normal curves are entirely contained in a huge variety of quadrics. Rational normal curves are Veronese varieties and, as such, they admit a projective generation. The latter fact may be used for a synthetic or constructive approach to G^k interpolation problems with ruled or channel surfaces.

The degree of \mathcal{B} and the type of the quadric \mathcal{Q} have to match. For example, on a two-dimensional (Euclidean) sphere we will never find real cubics.

4 Results and Algorithms

4.1 G^1 interpolation - common parabolic linear line congruence of surface tangents

We solve the G^1 interpolation problem on a quadric with a single cubic. However, we don't have to insert an additional control point (*i.e.*, a ruling or sphere) in between the two sets of boundary data and we get along with one interpolant in contrast to [26].

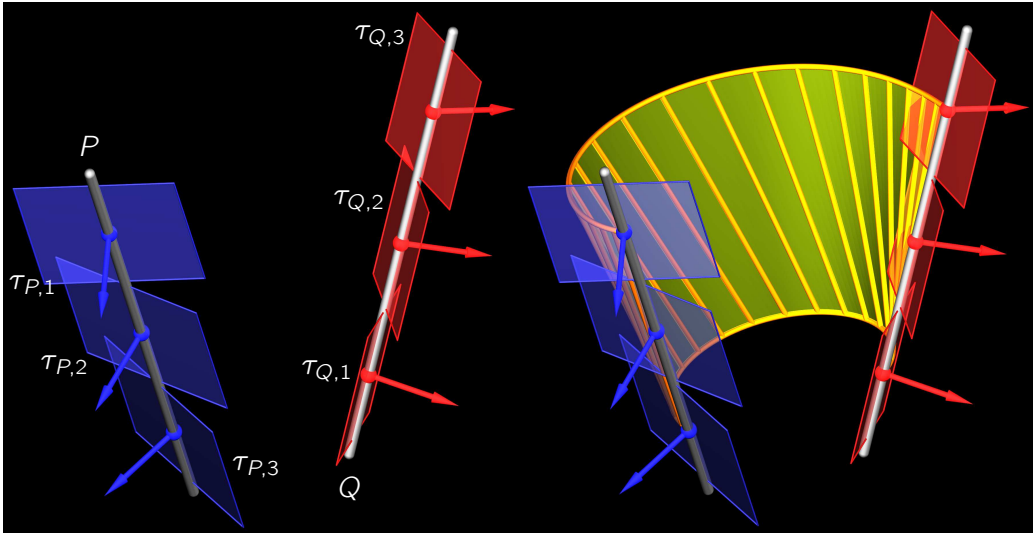


Figure 6: Left: G^1 ruled surface data consisting of rulings P , Q , and the tangent planes $\tau_{P,j}$, $\tau_{Q,i}$ ($i, j \in \{1, 2, 3\}$) along P and Q . Right: A ruled surface that interpolates the given G^1 data.

Unlike in the approach to G^1 interpolation given in [26], we do not have to take care of tangent planes at particular points on the boundary rulings. Since we are performing the interpolation solely in the quadric model of the present geometry, it is guaranteed that the *contact projectivities* at the rulings P and Q (*i.e.*, the boundaries) match.

If we let $n = 3$ in (8), we have to determine four control points B_0, \dots, B_3 (with coordinate vectors \mathbf{b}_i). The interpolant \mathcal{B} shall satisfy $\mathcal{B}(0) = P$, $\mathcal{B}(1) = Q$ at the ends which causes $B_0 = P$ and $B_3 = Q$, *i.e.*,

$$\mathbf{b}_0 = \mathbf{p}, \quad \mathbf{b}_3 = \mathbf{q}. \quad (11)$$

Along these bounding rulings, the parabolic linear line congruence of surface

tangents shall be determined by $[P, \dot{P}]$ and $[Q, \dot{Q}]$. Similarly, we can formulate this in terms of spheres. Consequently, the inner control points of the cubic Bézier curve \mathcal{B} have to be chosen such that $B_1 \in [P, \dot{P}]$ and $B_2 \in [Q, \dot{Q}]$ which, expressed in terms of vectors, reads

$$\mathbf{b}_1 = \lambda_1 \mathbf{p} + \mu_1 \dot{\mathbf{p}}, \quad \mathbf{b}_2 = \lambda_2 \mathbf{q} + \mu_2 \dot{\mathbf{q}} \quad (12)$$

where, in general, $\lambda_i : \mu_i \neq 0 : 0$ for $i \in \{1, 2\}$.

Now, $n = 3$ and (10) is a polynomial of degree 6 with seven coefficients. Since $P, \dot{P}, Q,$ and \dot{Q} fulfill (7), four coefficients vanish automatically and only three coefficients remain:

$$2\Omega_{0,2} + 3\Omega_{1,1} = 0, \quad 2\Omega_{1,3} + 3\Omega_{2,2} = 0, \quad \Omega_{0,3} + 9\Omega_{1,2} = 0. \quad (13)$$

Inserting (11) and (12) into (13), we arrive at

$$\begin{aligned} 2\lambda_2 \Omega_{p,q} + 2\mu_2 \Omega_{p,\dot{q}} + 3\mu_1^2 \Omega_{\dot{p},\dot{p}} &= 0, \\ 2\lambda_1 \Omega_{p,q} + 2\mu_1 \Omega_{\dot{p},q} + 3\mu_2^2 \Omega_{\dot{q},\dot{q}} &= 0, \\ \Omega_{p,q} + 9(\lambda_1 \lambda_2 \Omega_{p,q} + \lambda_1 \mu_2 \Omega_{p,\dot{q}} + \lambda_2 \mu_1 \Omega_{\dot{p},q} + \mu_1 \mu_2 \Omega_{\dot{p},\dot{q}}) &= 0. \end{aligned} \quad (14)$$

The first and second equation of (14) can be solved for λ_1 and λ_2 :

$$\lambda_1 = -\frac{\Omega_{\dot{p},q}}{\Omega_{p,q}} \mu_1 - \frac{3\Omega_{\dot{q},\dot{q}}}{2\Omega_{p,q}} \mu_2^2, \quad \lambda_2 = -\frac{\Omega_{p,\dot{q}}}{\Omega_{p,q}} \mu_2 - \frac{3\Omega_{\dot{p},\dot{p}}}{2\Omega_{p,q}} \mu_1^2, \quad (15)$$

provided that P and Q are not conjugate with respect to the quadric \mathcal{Q} (which is natural to assume). With (15) and the third equation of (14) we have a single equation

$$r : 81\Omega_{\dot{p},\dot{p}}\Omega_{\dot{q},\dot{q}}\mu_1^2\mu_2^2 + 36(\Omega_{p,q}\Omega_{\dot{p},\dot{q}} - \Omega_{p,\dot{q}}\Omega_{\dot{p},q})\mu_1\mu_2 + 4\Omega_{p,q}^2 = 0 \quad (16)$$

involving μ_1 and μ_2 describing a degenerate quartic curve in the $[\mu_1, \mu_2]$ -plane, see Fig. 7. The curve r is the union of a pair of hyperbolae and the points on it correspond to solutions of the G^1 interpolation problem.

Thus, we can formulate

Theorem 4.1. *G^1 Hermite data $D_0 = [P, \dot{P}]$ and $D_1 = [Q, \dot{Q}]$ satisfying (7) from a ruled or channel surface can be interpolated by a cubic ruled surface or a cubic one-parameter family of spheres and has two independent quadratic one-parameter families of solutions.*

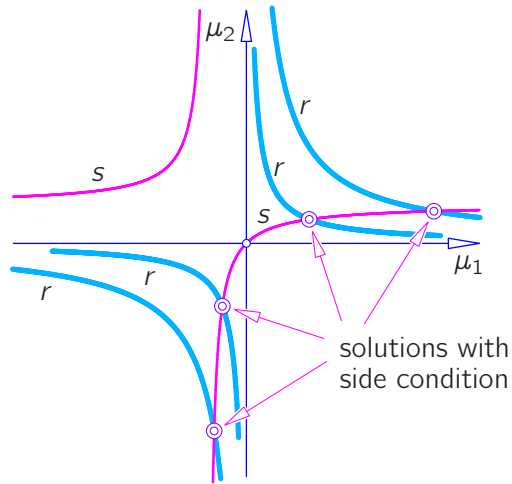


Figure 7: The degenerate quartic curve (16) consists of a pair of homothetic hyperbolae in the $[\mu_1, \mu_2]$ -plane. A non-linear side condition is imposed on the shape parameters μ_1, μ_2 in order to choose special solutions.

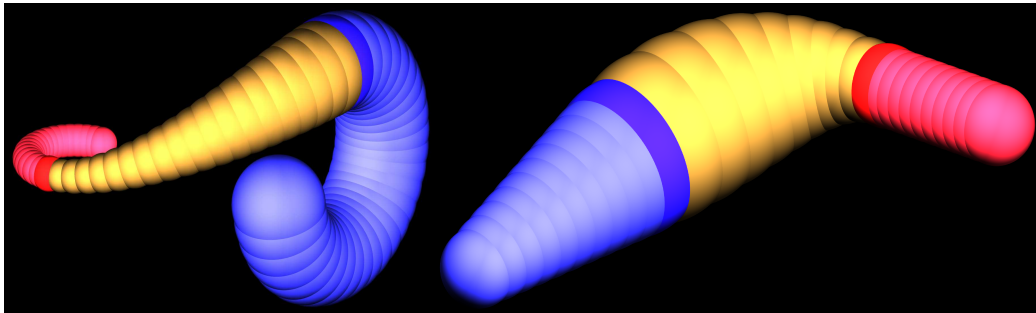


Figure 8: G^1 Hermite interpolation with one-parameter families of spheres.

In order to choose a certain solution in the G^1 problem, we can impose a side condition on the shape parameters μ_1 and μ_2 . This results in a further curve s in the $[\mu_1, \mu_2]$ -plane (cf. Fig. 7) and the computation of the solutions subject to this additional equation requires the intersection of r and s .

The case of the interpolation of channel surfaces somehow differs from that with ruled surfaces. In general, we cannot give a precise degree of the interpolating channel surface. However, the degree of the channel surface will not exceed 10 if the (cyclographic image of the) family of spheres is of degree 3. Figure 8 shows two examples of G^1 interpolation with channel surfaces: Only the spheres are plotted, since the interpolation algorithm is actually applied

to G^1 Hermite data of one-parameter families of spheres. In Figure 9, only the envelopes of the boundary channel surfaces and the interpolating channel surface of degree 10 are shown.

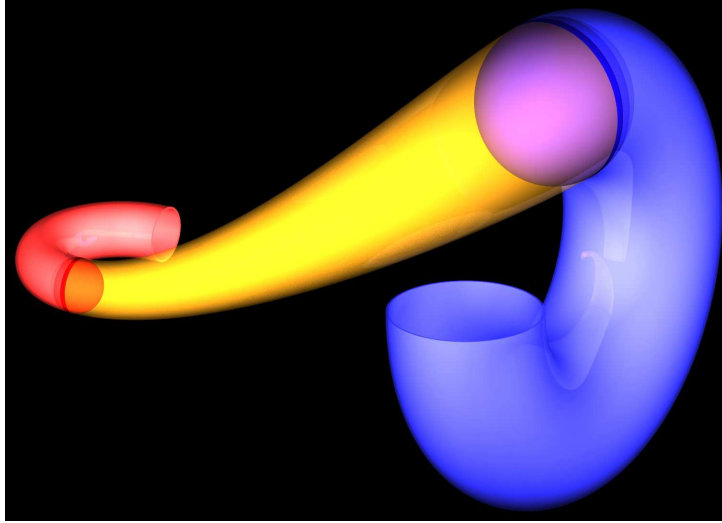


Figure 9: Envelopes of the families of spheres shown in Fig. 8 (left).

Improvements of the visualization of channel surfaces may be given in [1], although the results of our algorithms are presented sufficiently well.

4.2 G^2 interpolation - common osculating quadrics or Dupin cyclides

In the case of G^2 interpolation, the Hermite data $D_0 = [P, \dot{P}, \ddot{P}]$ and $D_1 = [Q, \dot{Q}, \ddot{Q}]$ contains information up to the second derivatives of the initial ruled or channel surface (see Fig. 10), and thus, also of the interpolant \mathcal{B} . Now, we assume that \mathcal{B} is given by (8) with $n = 5$.

The *endpoints* P, Q still have to be interpolated as well as the G^1 conditions still have to be fulfilled. Since now $n = 5$, (11) and (12) are valid in the G^2 case too and read

$$\begin{aligned} \mathbf{b}_0 &= \mathbf{p}, & \mathbf{b}_5 &= \mathbf{q}, \\ \mathbf{b}_1 &= \lambda_1 \mathbf{p} + \mu_1 \dot{\mathbf{p}}, & \mathbf{b}_4 &= \lambda_2 \mathbf{q} + \mu_2 \dot{\mathbf{q}} \end{aligned} \tag{17}$$

with $\lambda_i : \mu_i \neq 0 : 0$ for $i \in \{1, 2\}$. In order to obtain G^2 transitions at the boundaries P and Q , we have to make sure that the osculating planes of the

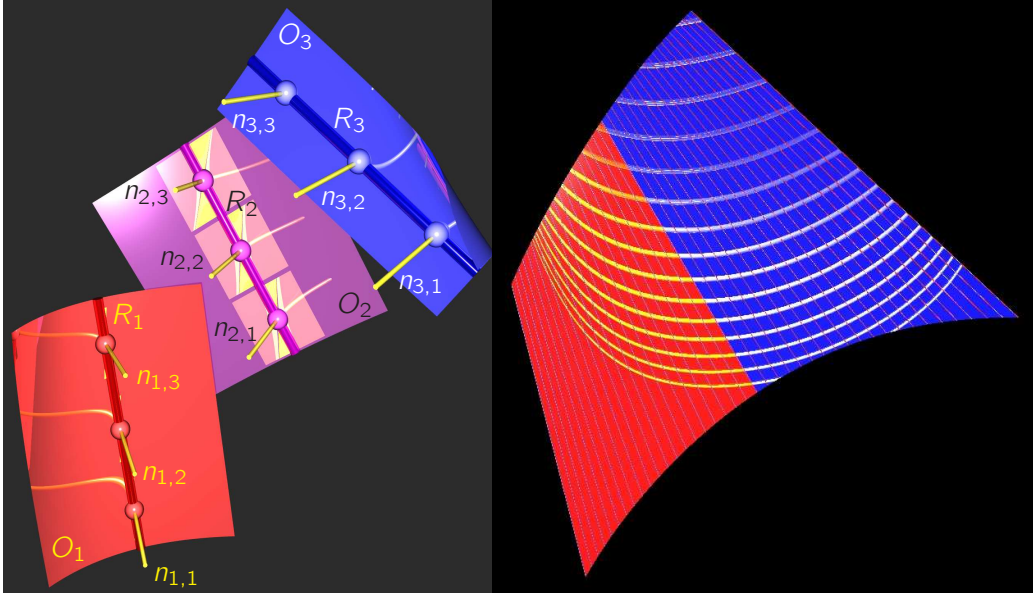


Figure 10: Left: G^2 ruled surface data consisting of rulings R_i , the prescribed tangent planes $\tau_{i,j}$ (with normals $n_{i,j}$), and the osculating reguli \mathcal{O}_i ($i, j \in \{1, 2, 3\}$). Right: Two ruled surfaces that interpolate the given G^2 data seen from the convex side with reflection lines.

interpolant agree with those of the initial curve. This is achieved by making sure that $B_2 \in [P, \dot{P}, \ddot{P}]$ and $B_3 \in [Q, \dot{Q}, \ddot{Q}]$ which means

$$\mathbf{b}_2 = \alpha_1 \mathbf{p} + \beta_1 \dot{\mathbf{p}} + \gamma_1 \ddot{\mathbf{p}}, \quad \mathbf{b}_3 = \alpha_2 \mathbf{q} + \beta_2 \dot{\mathbf{q}} + \gamma_2 \ddot{\mathbf{q}} \quad (18)$$

with $\alpha_i : \beta_i : \gamma_i \neq 0 : 0 : 0$ for $i \in \{1, 2\}$.

The condition (10) on \mathcal{B} to be entirely contained in M_2^4 is a polynomial of degree 10 with 11 coefficients. Since the identities given in (7) are valid, the coefficients of $(1-t)^{10}$, $t(1-t)^9$, $t^9(1-t)$, and t^{10} vanish automatically. Thus, seven coefficients remain and give that much conditions on the control points B_0, \dots, B_6 and the shape parameters of \mathcal{B} . So, we have

$$\begin{aligned} 4\Omega_{3i-3,3i-1} + 5\Omega_{3i-2,3i-2} &= 0, \\ \Omega_{2i-2,2i+1} + 5\Omega_{2i-1,2i} &= 0, \\ \Omega_{i-1,i+3} + 10\Omega_{i,i+2} + 10\Omega_{i+1,i+1} &= 0, \\ \Omega_{0,5} + 25\Omega_{1,4} + 100\Omega_{2,3} &= 0, \end{aligned} \quad i \in \{1, 2\}. \quad (19)$$

Inserting (17) and (18) into the first two equations of (19), we find

$$\gamma_i = -\frac{5}{4}\mu_i^2, \quad (i \in \{1, 2\}). \quad (20)$$

The partial solutions (20) are now inserted into (19) which are still linear in α_i . Therefore, they can be solved for α_i which yields

$$\begin{aligned}\alpha_2 &= -\frac{1}{\Omega_{p,q}} (\beta_2 \Omega_{p,\dot{q}} + \gamma_2 \Omega_{p,\ddot{q}} + 5\Omega_{\dot{p},\dot{p}} (\beta_1 \mu_1 - \gamma_1 \lambda_1) + 5\gamma_1 \mu_1 \Omega_{\dot{p},\dot{p}}), \\ \alpha_1 &= -\frac{1}{\Omega_{p,q}} (\beta_1 \Omega_{\dot{p},q} + \gamma_1 \Omega_{\ddot{p},q} + 5\Omega_{\dot{q},\dot{q}} (\beta_2 \mu_2 - \gamma_2 \lambda_2) + 5\gamma_2 \mu_2 \Omega_{\dot{q},\dot{q}}).\end{aligned}\quad (21)$$

Now, the three remaining equations involve only six variables: β_i , λ_i , and μ_i . The following list displays the degree of each equation considered as a polynomial in the respective variable:

$$\begin{aligned} & [[\beta_1, 2], [\beta_2, 1], [\lambda_1, 2], [\lambda_2, 1], [\mu_1, 4], [\mu_2, 3]], \\ & [[\beta_1, 1], [\beta_2, 2], [\lambda_1, 1], [\lambda_2, 2], [\mu_1, 3], [\mu_2, 4]], \\ & [[\beta_1, 1], [\beta_2, 1], [\lambda_1, 1], [\lambda_2, 1], [\mu_1, 3], [\mu_2, 3]].\end{aligned}\quad (22)$$

With two further elimination steps, we can eliminate two more variables from the latter equations. This shows that there is a three-dimensional algebraic variety of solutions to the G^2 Hermite interpolation problem. Each point on this variety corresponds to an interpolant of the given G^2 data.

For practical reasons, the huge variety of solutions shall be restricted. Since the parameters μ_1 and μ_2 regulate the influence of the first derivative, and therefore, the tangential behavior of the interpolant, one can make sure that they do not vanish by setting them to a fixed value. This has one major advantage: The degrees of three equations, simplified in (22) drop and, after eliminating λ_i , we obtain an algebraic curve of degree 6 in the $[\beta_1, \beta_2]$ -plane all of whose points correspond to solutions of the G^2 Hermite interpolation problem with ruled or channel surfaces. Summarizing, we can say:

Theorem 4.2. *The Hermite interpolation of G^2 data $D_0 = [P, \dot{P}, \ddot{P}]$ and $D_1 = [Q, \dot{Q}, \ddot{Q}]$ satisfying (7) from a ruled or channel surface can be solved with a quintic ruled surface or a quintic one-parameter family of spheres. The variety of solutions is algebraic, of dimension 3, and is at most of degree 150. With prescribed weights μ_i for the tangent points (derivate points) the manifold of solutions is an algebraic curve of degree 8.*

Remark: The degree 150 of the variety of solutions mentioned in Thm. 4.2 can (more or less) easily be verified by computing the Hilbert polynomial of the ideal defined by (22). In this case, the complexity of the computation was too high to carry it out by Maple[®]. The number 150 is an upper bound and is the product of the degrees of the equations given in (22) (according to Bézout's theorem).

Fig. 11 shows three different solutions to one certain G^2 interpolation task. It is no surprise that the interpolants intersect the osculating quadrics at the ends in more than just the common ruling. The interpolant and the osculating quadrics share only differential geometric properties up to order two.

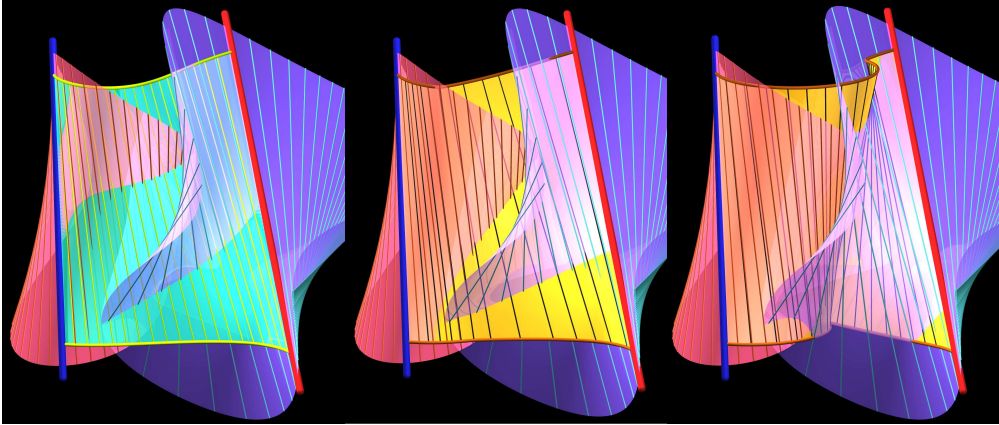


Figure 11: Three different solutions to a G^2 Hermite interpolation problem. The given reguli at the ends are shown in red and violet; the respective boundary lines show up as blue and red cylinders. It is not at all surprising that the three different interpolants (cyan, yellow, and orange) show some intersection curves with the G^2 data at the boundaries, since these surfaces only agree with the data up to differentiation order two.

In cases similar to that illustrated in Fig. 11, it is useful to have some tool which helps us to decide which solution is the *best*. Interpolants with small variations shall be preferred. Of course, solutions with self-intersections or even complicated topology should be omitted. Especially in the cases of G^2 (and later also G^3) interpolation, the shape parameters of the interpolants are solutions of systems of algebraic equations, and thus, they can only be found with numerical methods, in general. Then, the Bézier representation \mathcal{B} of the interpolant has numerically defined control points and this makes the solution somehow imprecise. Algebraically speaking, the polynomial $\rho(t) = \Omega(\mathcal{B}, \mathcal{B})$ will not be zero.

Fig. 12 shows the plot of the polynomials ρ corresponding to some solutions of a G^2 interpolation problem. Clearly, the *best* solution would be that corresponding to $\rho(t) \equiv 0$. However, in practice one chooses the solution corresponding to the polynomial $\rho(t)$ that is closest to the abscissa, at least in $[0, 1]$.

Fig. 13 shows a comparison of two solutions of a G^2 interpolation problem

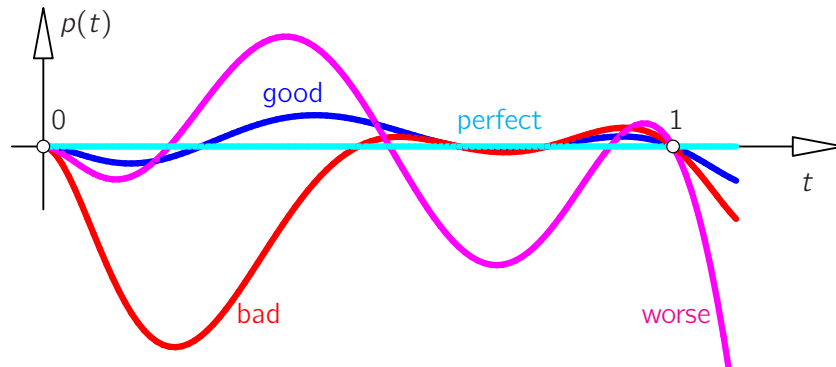


Figure 12: The polynomial $p(t)$ is not equal to zero for numerically obtained solutions. The solution corresponding to the polynomial function p closest to 0 is probably the best one.

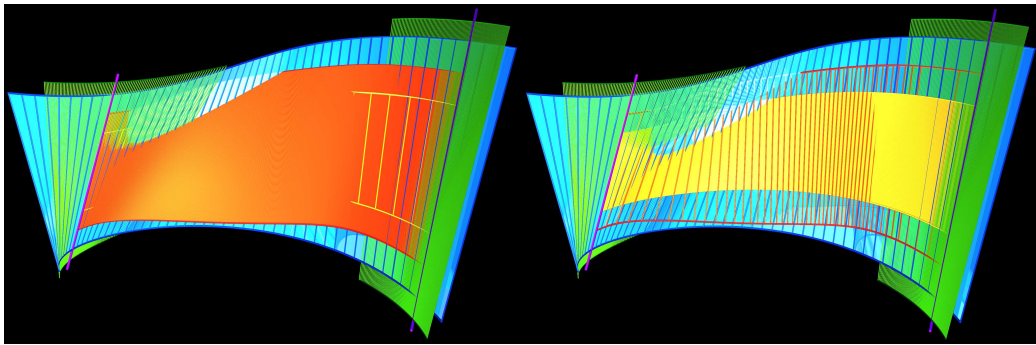


Figure 13: Comparison of two solutions of G^2 interpolation problem for ruled surfaces. The G^2 data was taken from the blue surface. The yellow and the orange solution have been chosen according to the deviations of the function $p(t)$ from the zero polynomial.

for ruled surfaces. We can still observe some intersections of the initial ruled surface (blue) and the interpolants (yellow, red) in Fig. 13. This is clear, since the interpolants computed from the G^2 data (green) agree with the initial surface (blue) only at the boundaries and to a certain extent.

The proposed algorithm also works for channel surfaces as can be seen in Fig. 14. There, two good solutions are displayed together with two bad solutions. In the latter case, we observe that the radius function may have zeros in the interval $[0, 1]$. This means that the orientation of the spheres in the one-parameter family changes. If this happens twice (an even number of changes), then both data sets at the ends are properly oriented (they have

equal orientations). Such cases can be treated relatively easy by adjusting the shape parameters μ_i . An odd number of zeros, or equivalently, an odd number of orientation switches, can be repaired by changing the orientation of the sphere at one of the two ends. If a solution looks pretty good and shows no

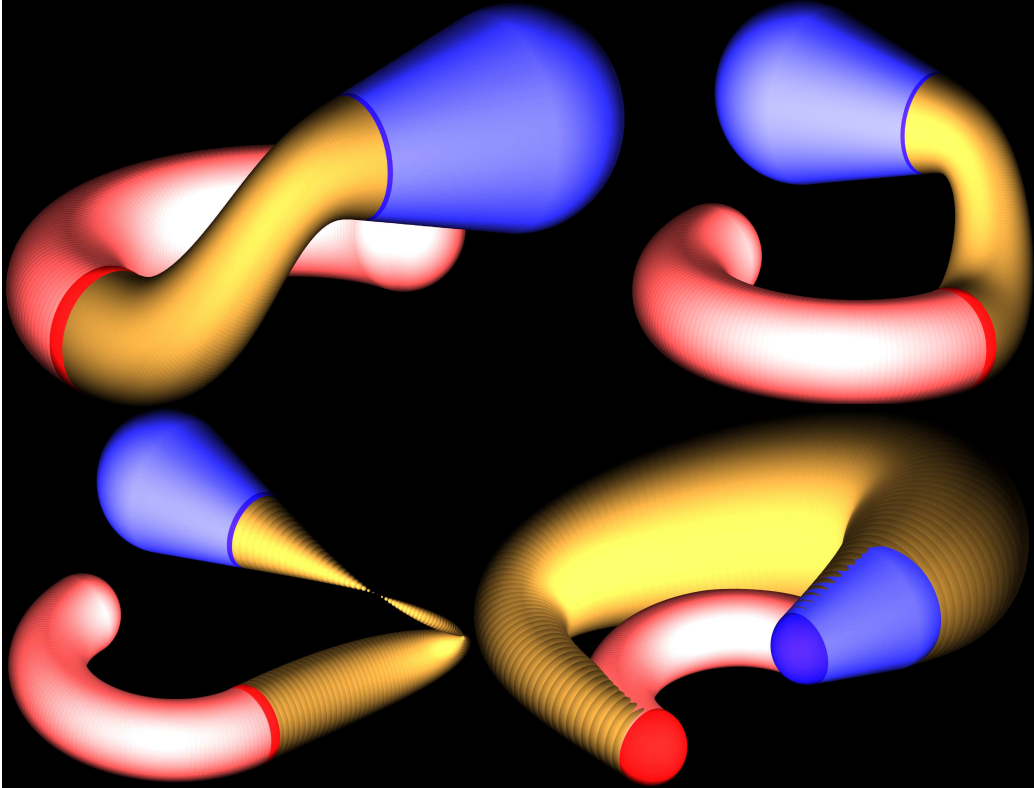


Figure 14: Top row: two good solutions of a G^2 interpolation problem with channel surfaces. Bottom row: two bad solutions with zeros of the radius function (left) or growth into the wrong direction (right).

zeros of the radius function, it may still grow into the wrong direction, see Fig. 13 (bottom row, right). This can be repaired by changing the signs of μ_i .

4.3 G^3 Hermite interpolation - common flecnodes

Finally, we pay attention to the interpolation of G^3 data $D_0 = [P, \dot{P}, \ddot{P}, \ddot{P}]$ and $D_1 = [Q, \dot{Q}, \ddot{Q}, \ddot{Q}]$. In this case, the interpolant does not only share the ruling or sphere P , the parabolic linear line or sphere congruence defined by $[P, \dot{P}]$, and the osculating regulus or Dupin cyclide defined by $[P, \dot{P}, \ddot{P}]$

with the ruled or channel surface to be interpolated. Among the asymptotic tangents or spheres of both ruled or channel surfaces along the common ruling or sphere P (and different from P), there are in general two lines or spheres which *hyperosculate* the ruled or channel surfaces, *i.e.*, locally they intersect the surfaces at least with multiplicity four. These two asymptotic lines or spheres are called *flecnodal tangents* or *flecnodal spheres*, [24, 30, 33].

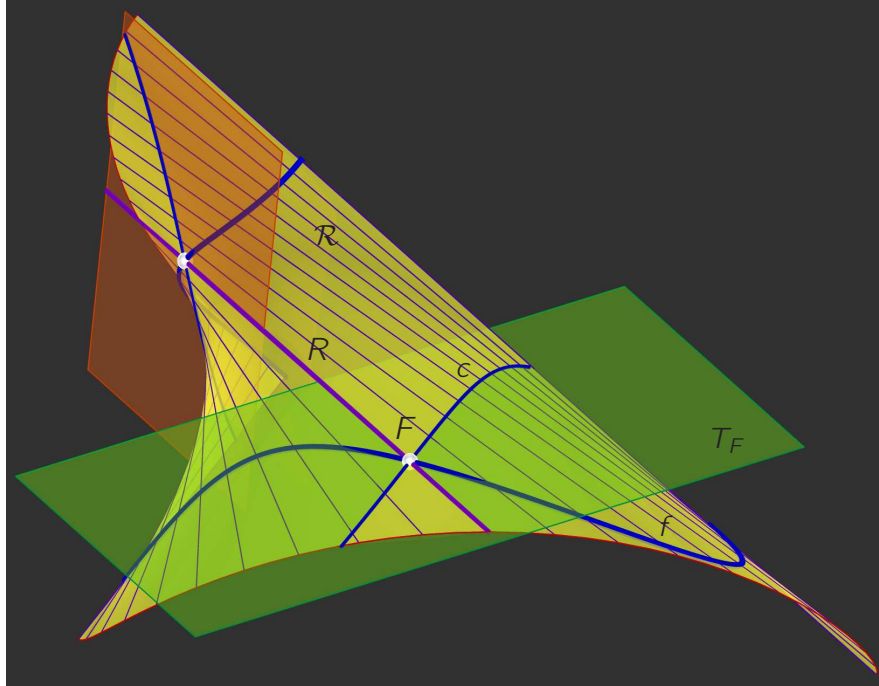


Figure 15: The tangent plane T_F at a flecnode F of a ruled surface \mathcal{R} intersects \mathcal{R} along the ruling R through F and a curve c with an inflection point at the flecnode F . The locus of all flecnodes on \mathcal{R} is the curve f consisting of two branches (at least in this example).

We have to choose $n = 7$ in (8) in order to have the necessary degrees of freedom, *i.e.*, the necessary number of control points. The relations between the control points and the derivative points at the boundary, similar to (11), (12), and (18) are

$$\begin{aligned}
 \mathbf{b}_0 &= \mathbf{p}, & \mathbf{b}_7 &= \mathbf{q}, \\
 \mathbf{b}_1 &= \lambda_1 \mathbf{p} + \mu_1 \dot{\mathbf{p}}, & \mathbf{b}_6 &= \lambda_2 \mathbf{q} + \mu_2 \dot{\mathbf{q}}, \\
 \mathbf{b}_2 &= \alpha_1 \mathbf{p} + \beta_1 \dot{\mathbf{p}} + \gamma_1 \ddot{\mathbf{p}}, & \mathbf{b}_5 &= \alpha_2 \mathbf{q} + \beta_2 \dot{\mathbf{q}} + \gamma_2 \ddot{\mathbf{q}}
 \end{aligned} \tag{23}$$

where $\lambda_i : \mu_i \neq 0 : 0$ and $\alpha_i : \beta_i : \gamma_i \neq 0 : 0 : 0$ for $i \in \{1, 2\}$. Additionally, we have to take the third derivatives at the boundaries into account. In

order to achieve a G^3 contact at P and Q , we make sure that the osculating three-spaces of the interpolant and the curves to be interpolated agree at the endpoints P and Q . Therefore, we have

$$\mathbf{b}_3 = \nu_1 \mathbf{p} + \omega_1 \dot{\mathbf{p}} + \rho_1 \ddot{\mathbf{p}} + \sigma_1 \dddot{\mathbf{p}}, \quad \mathbf{b}_4 = \nu_2 \mathbf{q} + \omega_2 \dot{\mathbf{q}} + \rho_2 \ddot{\mathbf{q}} + \sigma_2 \dddot{\mathbf{q}} \quad (24)$$

where $\nu_i : \omega_i : \rho_i : \sigma_i \neq 0 : 0 : 0 : 0$ for $i \in \{1, 2\}$. In analogy to (13) and (19), the coefficients of the polynomial (10) yield the eleven equations

$$\begin{aligned} 6\Omega_{5i-5,5i-3} + 7\Omega_{5i-4,5i-4} &= 0, \\ 5\Omega_{4i-4,4i-1} + 21\Omega_{4i-3,4i-2} &= 0, \\ 10\Omega_{3i-3,3i+1} + 70\Omega_{3i-2,3i} + 63\Omega_{3i-1,3i-1} &= 0, \\ 3\Omega_{2i-2,2i+3} + 35\Omega_{2i-1,2i+2} + 105\Omega_{2i,2i+1} &= 0, \\ 2\Omega_{i-1,i+5} + 42\Omega_{i,i+4} + 210\Omega_{i+1,i+3} + 175\Omega_{i+2,i+2} &= 0, \\ \Omega_{0,7} + 49\Omega_{1,6} + 441\Omega_{2,5} + 1225\Omega_{3,4} &= 0 \end{aligned} \quad (i \in \{1, 2\}) \quad (25)$$

since four coefficients vanish automatically. Because of (7), we have $\Omega_{0,0} = \Omega_{7,7} = \Omega_{0,1} = \Omega_{6,7} = 0$. So far, (25) involve 18 variables, *i.e.*, the homogeneous coordinates fixing the control points in the osculating subspaces together with the shape parameters. These 18 variables are subject to 11 conditions. From that we can infer that there is a seven-dimensional manifold of solutions to the G^3 interpolation problem.

We insert (23) and (24) into (25). The first two equations are univariate and linear in γ_i and can be solved for which gives

$$\gamma_i = \frac{7}{6} \mu_i^2 \quad (i \in \{1, 2\}) \quad (26)$$

since $\Omega_{\mathbf{p},\dot{\mathbf{p}}} = -\Omega_{\dot{\mathbf{p}},\mathbf{p}}$ and $\Omega_{\mathbf{q},\dot{\mathbf{q}}} = -\Omega_{\dot{\mathbf{q}},\mathbf{q}}$ according to (7). The third to sixth equation of (25) are four linear equations in ρ_i and σ_i ($i \in \{1, 2\}$) even after the substitution of (26). So, we solve the latter four equations for ρ_i, σ_i and substitute into the remaining equations. This yields five equations in twelve unknowns. There, we observe that the first two equations are linear in α_1 and α_2 , and thus, they can be solved for α_i which (after substitution for α_i) leads to three equations in ten unknowns still describing a seven-dimensional manifold of solutions. These three equations are all of the same algebraic shape, *i.e.*, they agree in the degree in total as well as in the degrees when considered as polynomials in certain variables:

$$[26, [\beta_i, 6], [\lambda_i, 6], [\mu_i, 16], [\nu_i, 2], [\omega_i, 2]] \quad (i \in \{1, 2\}).$$

The first number equals the total degree (it is 26).

Surprisingly, the latter three polynomial equations *all* share the same quadratic factor $c_1\lambda_1\lambda_2 + c_0$ with multiplicity two. On the doubly counted quadratic hypercylinder $\Gamma : c_1\lambda_1\lambda_2 + c_0 = 0$ in \mathbb{R}^{10} , we can for sure find a huge variety of real solutions to the G^3 interpolation problem on quadrics. Unfortunately, the complexity of the computation - the high degrees of the three final equations - forces us to restrict the manifold of solutions in practical cases. It means no restriction to set some of the shape parameters to certain fixed values, thereby guaranteeing that all derivative points contained in the boundary data have influence on the interpolant.

For example: Setting the parameters β_i , λ_i , and μ_i to certain fixed values and eliminating all remaining unknowns except ν_i yields an algebraic curve of degree 16 in the $[\nu_1, \nu_2]$ -plane all of whose points correspond to solutions to the initial G^3 interpolation problem in general. The solutions taken from the sextadecic differ from those corresponding to the points on the quadratic cylinder Γ . We can summarize:

Theorem 4.3. *The G^3 Hermite interpolation problem for ruled and channel surfaces can be done with septic curves on Plücker's or Lie's quadric. The solutions correspond to points on a seven-dimensional algebraic variety whose degree is at most $26^3 = 17576$.*

With prescribed weights β_i , λ_i , and μ_i the variety of solutions is an algebraic curve of degree 16.

Figure 16 shows three ruled surface patches glued together with G^3 continuity. The smoothness of the reflection lines of a spherical grid demonstrates the quality of the interpolation.

5 Conclusion and further ideas

5.1 C^1 instead of G^1 connections

In Sec. 1 (see page 1), we have foretold that a quartic curve can also be used for the interpolation of G^1 data on a quadric \mathcal{Q} . Moreover, even a C^1 join can be achieved. We use the well-known fact that the derivatives of a Bézier curve \mathcal{B} at both of its endpoints can be given in the simple form $\dot{\mathcal{B}}(0) = \Delta\mathbf{b}_1$ and $\dot{\mathcal{B}}(1) = \Delta\mathbf{b}_4$ where $\Delta\mathbf{b}_i = \mathbf{b}_i - \mathbf{b}_{i-1}$ is short hand for the *forward difference operator* applied to the i -th control point \mathbf{b}_i (see, e.g., [13]). Now, we have

$$\dot{\mathcal{B}}(0) = \dot{\mathbf{p}} = 4(\mathbf{b}_1 - \mathbf{b}_0), \quad \dot{\mathcal{B}}(1) = \dot{\mathbf{q}} = 4(\mathbf{b}_4 - \mathbf{b}_3),$$

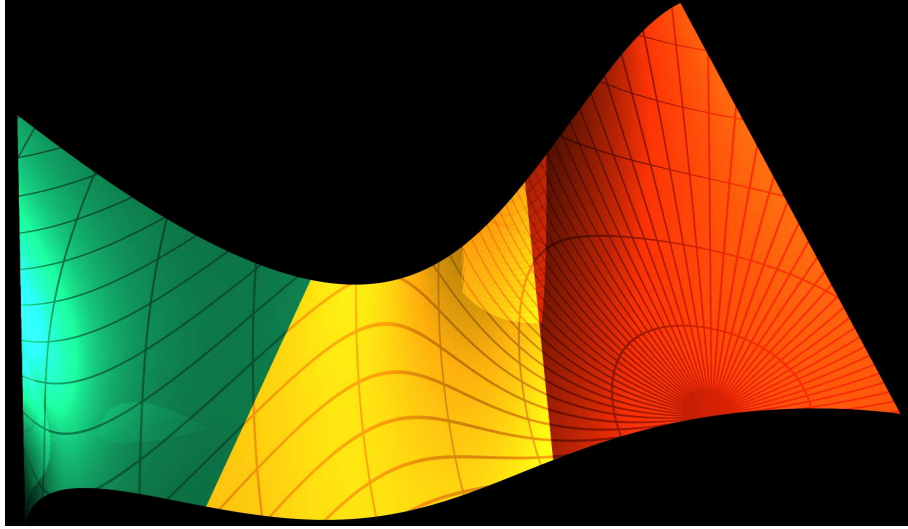


Figure 16: Three patches of ruled surfaces joined with third order geometric continuity. The fading grid of curves on the surface(s) is the reflection of a spherical grid.

and clearly $\mathcal{B}(0) = \mathbf{b}_0 = \mathbf{p}$ and $\mathcal{B}(1) = \mathbf{q} = \mathbf{b}_4$, and therefore, we find

$$\mathbf{b}_1 = \mathbf{p} + \frac{1}{4}\dot{\mathbf{p}} \quad \text{and} \quad \mathbf{b}_3 = \mathbf{q} - \frac{1}{4}\dot{\mathbf{q}}.$$

This particular choice of \mathbf{b}_0 , \mathbf{b}_1 , \mathbf{b}_3 , and \mathbf{b}_4 is necessary and sufficient for a C^1 connection of \mathcal{B} with two curves having G^1 data $D_0 = [\mathbf{p}, \dot{\mathbf{p}}]$ and $D_1 = [\mathbf{q}, \dot{\mathbf{q}}]$ at its endpoints since the derivative points of the Bézier curve agree with that of the given curve(s).

There is one control point left and we assume that $\mathbf{b}_2 = \mathbf{x} \in \mathbb{R}^6$. Then, (10) yields the following five equations

$$\begin{aligned} 3\Omega_{2i-1,2i} + 4\Omega_{2i-1,2i-1} &= 0, \quad \Omega_{i-1,i+2} + 6\Omega_{i,i+1} = 0, \quad i \in \{1, 2\}, \\ \Omega_{0,4} + 16\Omega_{1,3} + 36\Omega_{2,2} &= 0. \end{aligned}$$

The first four equations are linear in the coordinates of \mathbf{x} which, in general, describe a two-dimensional subspace of the affine space over \mathbb{R}^6 as the orbit of all possible X (or $\mathbf{x} = \mathbf{b}_2$). In total, we have the system of equations

$$\begin{aligned} 12\Omega_{\mathbf{p},\mathbf{x}} + \Omega_{\dot{\mathbf{p}},\dot{\mathbf{p}}} &= 0, \quad 12\Omega_{\mathbf{q},\mathbf{x}} + \Omega_{\dot{\mathbf{q}},\dot{\mathbf{q}}} = 0, \\ 4\Omega_{\mathbf{p},\mathbf{q}} - \Omega_{\mathbf{p},\dot{\mathbf{q}}} + 24\Omega_{\mathbf{p},\mathbf{x}} + 6\Omega_{\dot{\mathbf{p}},\mathbf{x}} &= 0, \quad 4\Omega_{\mathbf{p},\mathbf{q}} - \Omega_{\dot{\mathbf{p}},\mathbf{q}} + 24\Omega_{\mathbf{q},\mathbf{x}} - 6\Omega_{\dot{\mathbf{q}},\mathbf{x}} = 0, \\ 17\Omega_{\mathbf{p},\mathbf{q}} + 4(\Omega_{\dot{\mathbf{p}},\mathbf{q}} + \Omega_{\mathbf{p},\dot{\mathbf{q}}}) - \Omega_{\dot{\mathbf{p}},\dot{\mathbf{q}}} + \Omega_{\mathbf{x},\mathbf{x}} &= 0. \end{aligned}$$

Obviously, the solutions of the C^1 interpolation problem fill a one-dimensional quadratic variety (*i.e.*, a conic) in the quadric \mathcal{Q} (either L_2^4 or M_2^4). That is definitely less than in the more flexible cubic ansatz given in (11) and (12). Unfortunately, the reality of solutions cannot be guaranteed in this case.

5.2 Channel surfaces and the cyclographic model

The interpolation with channel (or even pipe) surfaces should preferably be done within the cyclographic model (cf. [9, 21]). There, the interpolation task simplifies to a linear G^k spline interpolation. The solutions to prescribed boundary data will be of low degree and unique. The latter may be seen as a minor flaw.

However, one problem still persists: The interpolation in the cyclographic model yields a G^k curve corresponding to a G^k family of spheres. The computation of the envelope consumes one degree of smoothness and so the resulting channel surface shows only a G^{k-1} continuity at the boundaries.

5.3 Torsal interpolants

The presented algebraic approach to the interpolation in quadrics could also be used for finding interpolating torsal ruled surfaces. Therefore, the parametrization \mathcal{B} of the interpolant has to fulfill $\Omega(\mathcal{B}, \mathcal{B}) \equiv 0$ in addition to (10). The number of conditions imposed on the fixed number of shape parameters increases and in each case we have to clarify if the chosen degree of the ansatz is sufficiently high.

5.4 Further possible applications

The presented interpolation method on quadrics could also be used for families of circles in the plane, no matter if the plane is Euclidean or pseudo-Euclidean. A stereographic projection to a Euclidean or pseudo-Euclidean sphere establishes the quadric model and the techniques apply.

Our technique can also be used to find exact parametrizations of interpolating motions since Study's quadric S_2^6 serves as a point model for the manifold of motions in Euclidean three-space, see [31]. A detailed study of the behavior of polynomial curves on S_2^6 is needed, especially the relative position of the osculants with respect to the quadric's three-dimensional generators.

5.5 Conclusion

We have presented a unifying treatment of the G^k Hermite interpolation within quadrics. The method was tested at hand of two special geometries: the geometries of lines and spheres. This was done not only since these are apparently of more practical relevance than others. These geometries are understood much better than others. Nevertheless, the results given in Thms. 4.1 – 4.3 are formulated in the general setting of an arbitrary (possibly) regular quadric. Therefore, they contain general results on the G^k Hermite interpolation by means of polynomial curves within quadrics.

References

- [1] A. Bienert: *Visualisierung und graphische Anwendung von Kanalflächen*. PhD thesis, Martin-Luther-Universität, Halle-Wittenberg, 2016.
- [2] B. Blaschitz: *Skinning of Circles and Spheres by Geometric Optimization in Minkowski Space* J. Geom. Graphics **18**/2 (2014), 159–172.
- [3] W. Blaschke: *Vorlesungen über Differentialgeometrie III*. Springer-Verlag, Berlin, 1929.
- [4] W. Burau: *Mehrdimensionale projektive und höhere Geometrie*. VEB Deutscher Verlag der Wissenschaften, Berlin, 1961.
- [5] T.E. Cecil: *Lie sphere geometry*. Springer, New York; 2nd ed. 2008.
- [6] R. Dietz, J. Hoschek, B. Jüttler: *An algebraic approach to curves and surfaces on the sphere and on other quadrics*. Comp. Aided Geom. Design **10** (1993), 211–229.
- [7] R.T. Farouki: *Pythagorean-Hodograph Curves: Algebra and Geometry Inseparable*. Springer, Berlin, 2008.
- [8] A. Gfrerrer: *Rational interpolation on a hypersphere*. CAGD **16**/1 (1999), 21–37.
- [9] O. Giering: *Vorlesungen über höhere Geometrie*. Vieweg, Braunschweig - Wiesbaden, 1982.
- [10] V. Hlavaty: *Projektive Liniengeometrie*. Noordhoff, Groningen, 1953.

- [11] J. Hoschek: *Liniengeometrie*. Bibliographisches Institut, Zürich, 1971.
- [12] J. Hoschek: *Bézier Curves and Surface Patches on Quadrics*. In: *Mathematical Methods in CAGD II*: Biri, Norway, 1991, T. Lyche, L.L. Schumaker (eds.), Vanderbilt Univ. Press, Nashville, 1992, 331–342.
- [13] J. Hoschek, D. Lasser: *Fundamentals of Computer Aided Geometric Design*. A.K. Peters, Wellesley, MA, 1993.
- [14] J. Hoschek, M. Schneider: *Interpolation and approximation with developable surfaces*. In: *Curves and Surfaces with Applications in CAGD*, A. Le Méhauté, C. Rabut, and L.L. Schumaker, (eds.), Vanderbilt University Press, Nashville, TN, 1997, 185–202.
- [15] J. Hoschek, U. Schwanecke: *Interpolation and approximation with ruled surfaces*. In: *The Mathematics of Surfaces VIII*, R. Cripps (ed.), Information Geometers, 1998, 213–231.
- [16] B. Jüttler: *Zur Konstruktion rationaler Kurven und Flächen auf Quadriken*. *J. Geometry* **47** (1993), 53–64.
- [17] R. Krasauskas: *Minimal rational parametrizations of channel surfaces*. *Computing* **79**/2–4, 281–290.
- [18] J. Lang, O. Röschel: *Developable $(1, n)$ -Bézier surfaces*. *Comput. Aided Geom. Design* **9** (1992), 291–298.
- [19] S. Leopoldseder: *Cone spline surfaces and spatial arc splines*. PhD thesis, Vienna University of Technology, 1998.
- [20] C. Mäurer, R. Krasauskas: *Joining cyclide patches along quartic boundary curves*. *Mathematical methods for curves & surfaces II*. M. Dæhlen, T. Lyche, L.L. Schumacher (eds.), Vanderbilt Univ. Press, Nashville, TN, 1998, 359–366.
- [21] E. Müller: *Vorlesungen über Darstellende Geometrie*. Band II: Die Zyklographie, Deuticke, Leipzig - Wien, 1929.
- [22] E. Müller, J.L. Krames: *Vorlesungen über Darstellende Geometrie*. Band III: Konstruktive Behandlung der Regelflächen. Deuticke, Leipzig - Wien, 1931.
- [23] B. Odehnal: *Subdivision algorithms for ruled surfaces*. *J. Geom. Graphics* **12**/1 (2008), 35–52.

- [24] B. Odehnal: *Note on flecnodes*. J. Geom. Graphics **13**/1 (2009), 29–40.
- [25] M. Peternell, H. Pottmann: *Computing rational parametrizations of channel surfaces*. J. Symbolic Computation **23** (1997), 255–266.
- [26] M. Peternell: *G^1 -Hermite Interpolation of Ruled Surfaces*. In: Mathematical Methods in CAGD, Oslo 2000, T. Lyche and L.L. Schumaker (eds.), Vanderbilt Univ. Press, Nashville, TN, 2001, 413–422.
- [27] M. Peternell: *Developable surface fitting to point clouds*. Comp. Aided Geom. Design **21** (2004), 785–803.
- [28] M. Peternell: *Recognition and reconstruction of developable surfaces from point clouds*. Proc. Geometric Modeling and Processing 2004, Beijing, China, 301–310.
- [29] H. Pottmann, G. Farin: *Developable rational Bezier and B-spline surfaces*. Comput. Aided Geom. Design **12** (1995), 513–531.
- [30] R. Sauer: *Projektive Liniengeometrie*. W. de Gruyter, Berlin, 1937.
- [31] E.A. Weiss: *Einführung in die Liniengeometrie und Kinematik*. B.G. Teubner, Leipzig, 1935.
- [32] E.A. Weiß: *Die geschichtliche Entwicklung der Lehre von der Geraden-Kugel-Transformation VII*. Deutsche Math. **3** (1938), 11–35.
- [33] K. Zindler: *Liniengeometrie mit Anwendungen*. Vol. I & II, G.J. Göschen'sche Verlagshandlung, Leipzig, 1906.